

1 'Premier' evidence for prolonged kimberlite pipe formation
2 and its influence on diamond transport from deep Earth

3 Sebastian Tappe^{1,*}, Ashish Dongre¹, Chuan-Zhou Liu², Fu-Yuan Wu²

4 ¹*Department of Geology, University of Johannesburg, P.O. Box 524, 2006 Auckland Park,*
5 *South Africa*

6 ²*State Key Laboratory of Lithospheric Evolution, Institute of Geology and Geophysics,*
7 *Chinese Academy of Sciences, 100029 Beijing, China*

8

9

10

11

12

13

14 ***Corresponding author (S.Tappe):** Department of Geology, University of Johannesburg, P.O.
15 Box 524, 2006 Auckland Park, Gauteng, South Africa; Tel: +27-011-5594733; Fax: +27-011-
16 5594702; E-mail: sebastiant@uj.ac.za

17

18 Table DR1 and DR2

19 **Supplementary File 1**

20 **Methods and Materials**

21 **Sample acquisition and preparation**

22 The kimberlite samples investigated during this study were obtained in 2016 by the senior
23 author over the course of several visits to the underground extension of Cullinan Diamond
24 Mine (Gauteng, South Africa). At the University of Johannesburg, the freshest samples were
25 cut into centimetre thick slabs with a rock saw, and all surficial crusts were removed and
26 discarded. Small blocks were reserved for each kimberlite sample for preparation of polished
27 petrographic thin sections at 25 μm thickness (University of Johannesburg). The kimberlite
28 slabs were thoroughly washed under running water, and only material visibly free of crustal
29 and mantle rock fragments was further processed. The contamination-screened kimberlite
30 slabs (approximately 500 to 800 grams per sample) were then wrapped in thick plastic bags
31 and crushed with a hammer into mm-sized rock chips (<8 mm). The kimberlite chips were
32 again contamination-screened and approximately 200 grams per sample were then processed
33 in an automated agate mill at the University of Johannesburg to obtain analytical grade rock
34 powder. The remaining 300 to 600 grams of kimberlite chips were processed by High-
35 Voltage-Pulse-Power-Fragmentation (SELFRAG) at the University of Pretoria to ensure non-
36 abrasive mineral liberation of the <1 mm grain size fractions. These fractions were further
37 sieved to collect grains within the target size range between 75 and 150 μm . The 75-150 μm
38 grain size fractions were then processed through a Frantz isodynamic separator, and the
39 obtained non-magnetic fractions were prepared for heavy liquid mineral separation at the

40 University of Johannesburg. The use of methylene iodide (diiodomethane) heavy liquid with a
41 density of ~3.33 g/ml at 25°C proved to be most successful for concentrating abundant
42 euhedral perovskite crystals (mainly resorbed octahedrons) from the fine-grained groundmass
43 of kimberlite. Five kimberlite samples were most suitable for our high-precision
44 geochronology study, and approximately 100 perovskite crystals per sample were mounted
45 (Figure DR4), together with grains of two mineral standards (Tazheran-3 and Afrikanda-5
46 perovskite), into a single epoxy puck (Mount# A4242). After polishing of the epoxy puck all
47 exposed crystals were inspected under a Cameca SX100 electron microprobe in BSE mode to
48 identify at least 20 crystals that are most suitable for SIMS spot analysis; i.e., inclusion and
49 zonation free (Figure DR4; see below).

50 **Electron microprobe analysis (EPMA)**

51 Fully quantitative major and minor element compositions of rock-forming minerals were
52 determined in situ on polished petrographic thin sections of the kimberlite dykes with a
53 Cameca SX100 electron microprobe at the University of Johannesburg. Optimal conductivity
54 of the thin sections was achieved with 25 nm thick carbon layers produced under vacuum in a
55 Quorum Q300T ES coater. The instrument was operated at an acceleration voltage of 20 kV
56 and a beam current of 20 nA. The electron beam was adjusted daily and optimized for 1 µm
57 spot analysis. Counting time varied between 12 and 40 s on peak, depending on the chemical
58 element. During phlogopite analysis, F and Cl were measured for 50 and 30 s on peak,
59 respectively. The electron microprobe was calibrated using the following natural and synthetic
60 international reference materials: diopside (Si), almandine garnet (Al), hematite (Fe),
61 wollastonite (Ca), olivine (Mg), rhodonite (Mn), orthoclase (K), jadeite (Na), fluorite (F), and

62 halite (Cl), as well as pure TiO₂, Cr₂O₃, and NiO. All elements of interest were measured on
63 their X-ray K α lines utilizing four wavelength dispersive spectrometers. Data reduction and
64 matrix correction was done applying the 'X-PHI' method, which is a $\phi(\rho z)$ -type off-line
65 analytical protocol.

66 **X-ray fluorescence analysis (XRF) and CO₂ determination**

67 The bulk rock major and minor element compositions of the kimberlite dykes were analyzed
68 using a PANalytical MagiX PRO X-ray fluorescence spectrometer at the University of
69 Johannesburg ([Table DR1](#)). Rock powders of <20 μm grain size were dried in an oven at
70 105°C prior to fusion into glass discs with the aid of a Li₂B₄O₇-LiBO₂ flux (50/50). In
71 addition, a small amount of LiBr was added to the flux to avoid stickiness between the
72 produced glass discs and the platinum moulds. The lower limit of detection for all elements of
73 interest is approximately 0.05 wt.%. Instrument calibration was conducted using mixtures of
74 pure metal oxides, and the accuracy of the XRF method was monitored by analysis of
75 certified reference materials (BE-N, JSy-1, SARM-2, SARM-16), as well as of in-house
76 carbonatite standards (ST199 and ST220II). For the in-house carbonatite standards, all major
77 and minor elements reported in [Table DR1](#) reproduced within 2% of the values reported in
78 [Tappe et al. \(2006\)](#).

79 Loss on ignition (LOI) was determined for all bulk rock powders at the University of
80 Johannesburg after heating of the samples to 930°C in air and holding at this temperature for
81 30 minutes. Bulk rock CO₂ contents were determined by liberation of CO₂ gas from the

82 sample powders in a reaction with 15% HClO₄ and subsequent photo-coulometry analysis,
83 with a lower limit of detection of 0.02 wt.% CO₂ (AcmeLabs, Bureau Veritas Group).

84 **U/Pb perovskite age determinations by Secondary Ion Mass Spectrometry (SIMS)**

85 The U/Pb perovskite isotope analyses were performed on a Cameca IMS-1280 ion-
86 microprobe mass spectrometer at the Institute of Geology and Geophysics, Chinese Academy
87 of Sciences, Beijing (IGGCAS). The U/Pb data for groundmass perovskites from four
88 kimberlite dykes (CIM15-72, CIM15-74, CIM15-76, CIM15-80) and a massive volcanoclastic
89 kimberlite unit (CIM15-83; 'Grey' kimberlite) of the Premier/Cullinan pipe are listed in **Table**
90 **DR2**, and displayed in **Figure 2** and online in **Figures DR2** and **DR5**. BSE images of polished
91 thin sections of kimberlite samples for which geochronology data were obtained are shown in
92 **Figure DR4** to document perovskite crystals in petrographic context. The complete dataset,
93 including the analyzed Afrikanda-5 perovskite mineral standard, is provided in **Table DR2**.

94 [Li et al. \(2010\)](#) provided a detailed account of the SIMS U/Pb isotope analytical protocol for
95 perovskite at IGGCAS in Beijing, and the following description is only a brief method
96 summary. The O²⁻ primary ion beam was accelerated at 13 kV, with 10 to 18 nA intensity.
97 Analysis spot size was approximately 20×30 μm. Positive secondary ions were extracted with
98 a 10 kV potential. For each sample, between 11 and 23 fresh euhedral and inclusion-free
99 perovskite grains (75-100 μm across) were analysed. Each spot analysis on a single perovskite
100 crystal consisted of 10 cycles, and data were collected for 16 minutes per grain. The U-Th-Pb
101 isotope ratios and elemental abundances of sample and secondary standard grains were
102 calibrated against the Tazheran-3 perovskite standard with a TIMS-determined ²⁰⁶Pb/²³⁸U age

103 of 463 ± 2 Ma (Kinny et al., 1997). This primary matrix-matched calibration standard was
104 measured at the beginning and at the end of the analytical session on 11/12 May 2017, as well
105 as after every three 'unknown' perovskite crystals. The U/Pb ages reported in Table DR2
106 were calculated with Isoplot 2.2 (Ludwig, 2000) using the decay constants recommended in
107 Steiger and Jäger (1977): $9.8485 \times 10^{-10} \text{ a}^{-1}$ for ^{235}U and $1.55125 \times 10^{-10} \text{ a}^{-1}$ for ^{238}U . The
108 presence of initial common Pb was corrected utilizing the measured amount of ^{204}Pb and the
109 terrestrial Pb evolution model of Stacey and Kramers (1975). It should be noted that the Pb
110 isotopic compositions of the Stacey and Kramers (1975) model between 1.1 and 1.15 Ga are
111 very similar to those of galena crystals recovered from the Premier kimberlite (Allsopp et al.,
112 1967). However, provided that the measured galena Pb isotopic compositions show
113 significant heterogeneity (i.e., $^{206}\text{Pb}/^{204}\text{Pb}$ range from 15.3 to 16.2), application of the Stacey
114 & Kramers model for initial common Pb correction is preferred. In general, we report final
115 U/Pb perovskite results as $^{206}\text{Pb}/^{238}\text{U}$ ages, because this decay scheme is less sensitive to the
116 common Pb correction, which can be significant for perovskite analyses (Heaman, 1989;
117 Kinny et al., 1997; Tappe and Simonetti, 2012).

118 The following age result for the Afrikanda-5 perovskite mineral standard for which 13 grains
119 were analyzed as unknowns during the analytical session on 11/12 May 2017 were obtained
120 (all uncertainties are reported at the 2-sigma level; see Table DR2 and Figure DR3):

121 $^{206}\text{Pb}/^{238}\text{U}$ age of 383.5 ± 3.0 Ma (recommended TIMS-determined $^{206}\text{Pb}/^{238}\text{U}$ age: 381.6 ± 1.4
122 Ma; Wu et al., 2013).

123

Publisher: GSA

Journal: Geology

DOI: 10.1130/G45097.1

124 **REFERENCES CITED**

- 125 Allsopp, H. L., Burger, A. J., and van Zyl, C., 1967, A minimum age for Premier kimberlite
126 pipe yielded by biotite Rb-Sr measurements with related galena isotopic data: *Earth*
127 *and Planetary Science Letters*, v. 3, p. 161–166.
- 128 Heaman, L. M., 1989, The nature of the subcontinental mantle from Sr-Nd-Pb isotopic studies
129 on kimberlitic perovskite: *Earth and Planetary Science Letters*, v. 92, no. 3-4, p. 323-
130 334.
- 131 Kinny, P. D., Griffin, B. J., Heaman, L. M., Brakhfogel, F. F., and Spetsius, Z. V., 1997,
132 SHRIMP U-Pb ages of perovskite from Yakutian kimberlites, *in* Sobolev, N. V., and
133 Mitchell, R. H., eds., *Proceedings of the Sixth International Kimberlite Conference*,
134 Volume 1: New York, United States, Allerton Press, p. 97-105.
- 135 Li, Q. L., Li, X. H., Liu, Y., Wu, F.-Y., Yang, J. H., and Mitchell, R. H., 2010, Precise U-Pb
136 and Th-Pb age determination of kimberlitic perovskites by secondary ion mass
137 spectrometry: *Chemical Geology*, v. 269, no. 3-4, p. 396-405.
- 138 Ludwig, K. R., 2000, *Isoplot/Ex version 2.2: A geochronological toolkit for Microsoft Excel:*
139 *Berkeley Geochronology Center Special Publication No. 1a*, p. Berkeley, California.
- 140 Stacey, J. S., and Kramers, J. D., 1975, Approximation of terrestrial lead isotope evolution by
141 a two-stage model: *Earth and Planetary Science Letters*, v. 26, no. 2, p. 207-221.
- 142 Steiger, R. H., and Jäger, E., 1977, Subcommittee on geochronology: Convention on the use
143 of decay constants in geo- and cosmochronology: *Earth and Planetary Science Letters*,
144 v. 36, no. 3, p. 359-362.
- 145 Tappe, S., Foley, S. F., Jenner, G. A., Heaman, L. M., Kjarsgaard, B. A., Romer, R. L.,
146 Stracke, A., Joyce, N., and Hoefs, J., 2006, Genesis of ultramafic lamprophyres and
147 carbonatites at Aillik Bay, Labrador: A consequence of incipient lithospheric thinning
148 beneath the North Atlantic craton: *Journal of Petrology*, v. 47, no. 7, p. 1261-1315.
- 149 Tappe, S., and Simonetti, A., 2012, Combined U-Pb geochronology and Sr-Nd isotope
150 analysis of the Ice River perovskite standard, with implications for kimberlite and
151 alkaline rock petrogenesis: *Chemical Geology*, v. 304-305, p. 10-17.
- 152 Wu, F.-Y., Arzamastsev, A. A., Mitchell, R. H., Li, Q. L., Sun, J., Yang, Y. H., and Wang, R.
153 C., 2013, Emplacement age and Sr–Nd isotopic compositions of the Afrikanda
154 alkaline ultramafic complex, Kola Peninsula, Russia: *Chemical Geology*, v. 353, p.
155 210-229.

156

Figure DR1

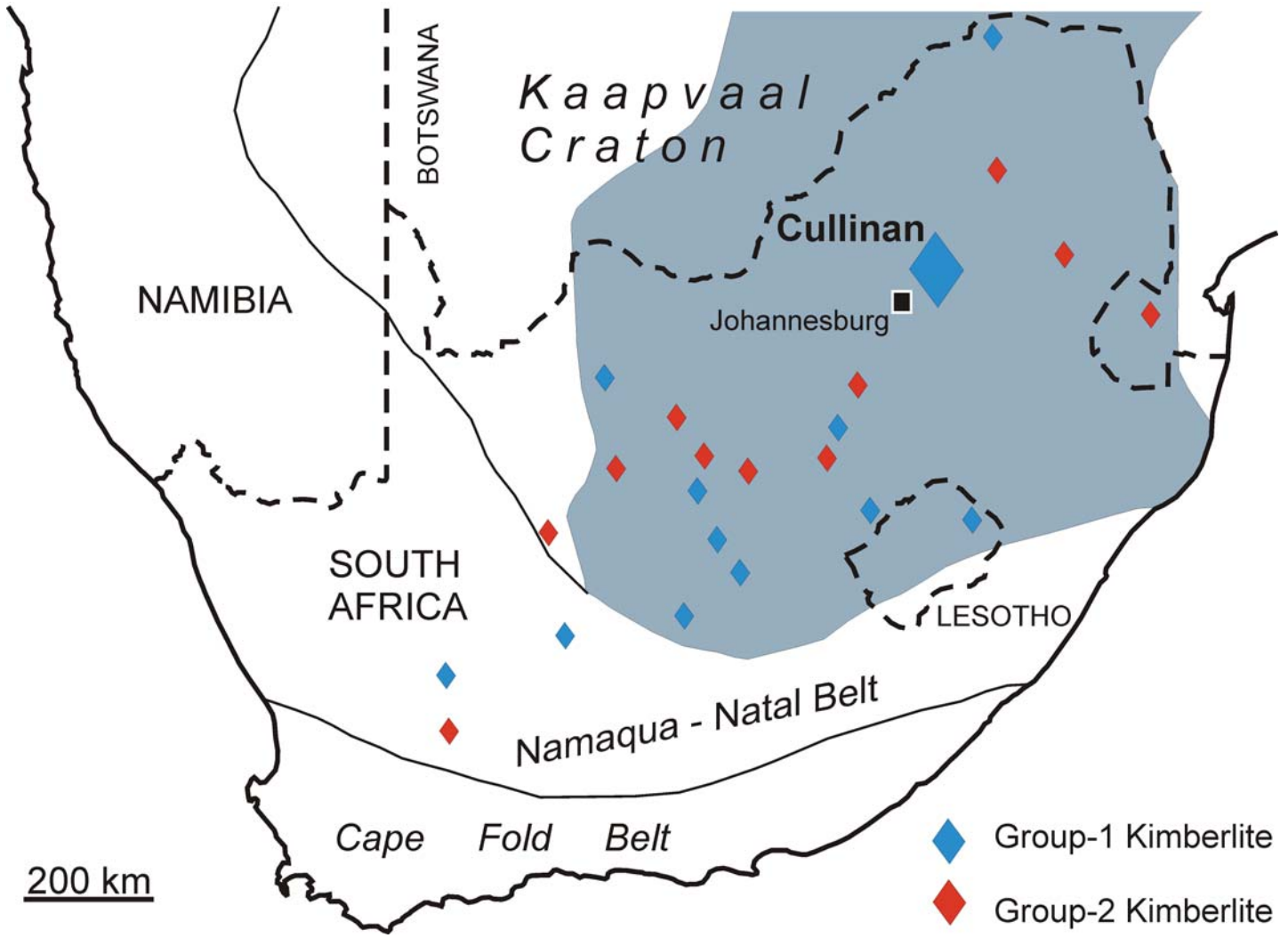


Figure DR2

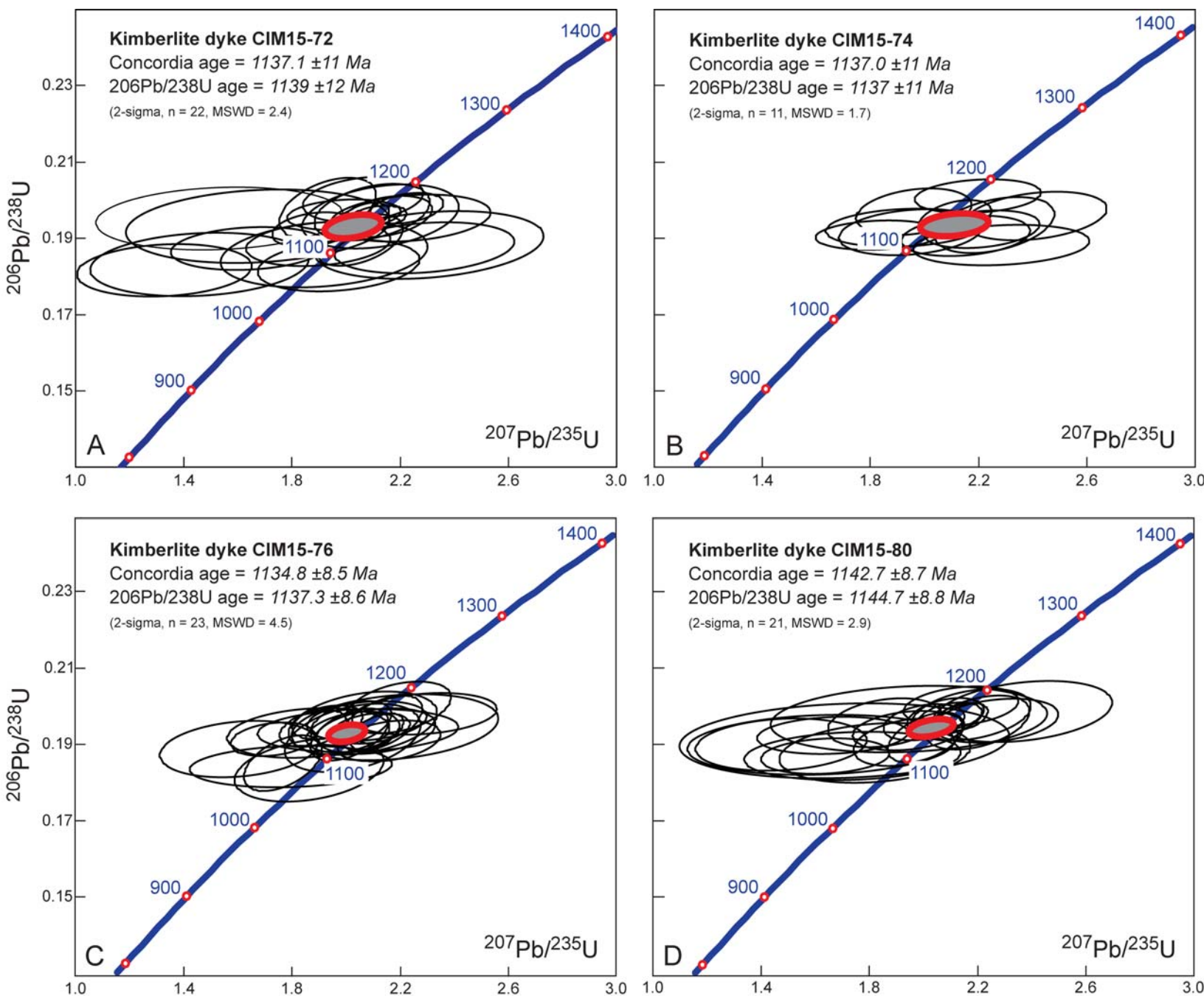
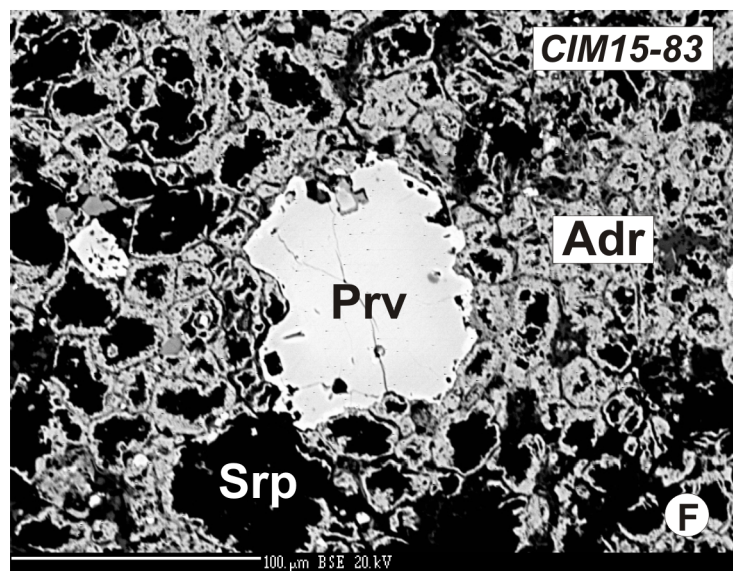
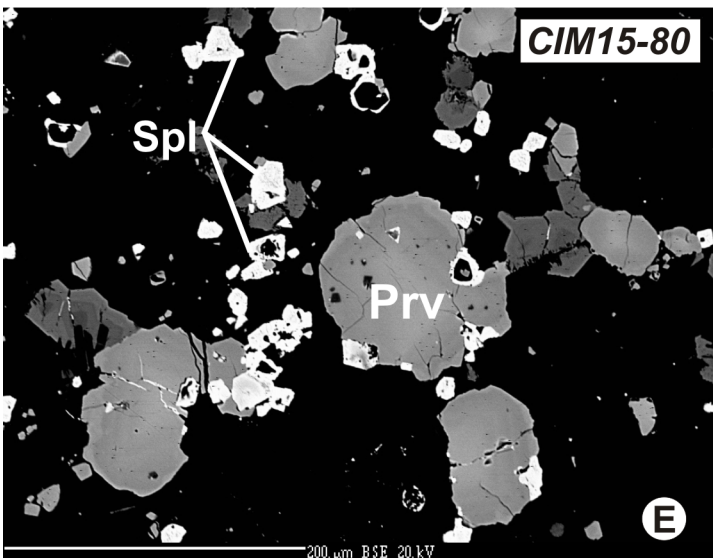
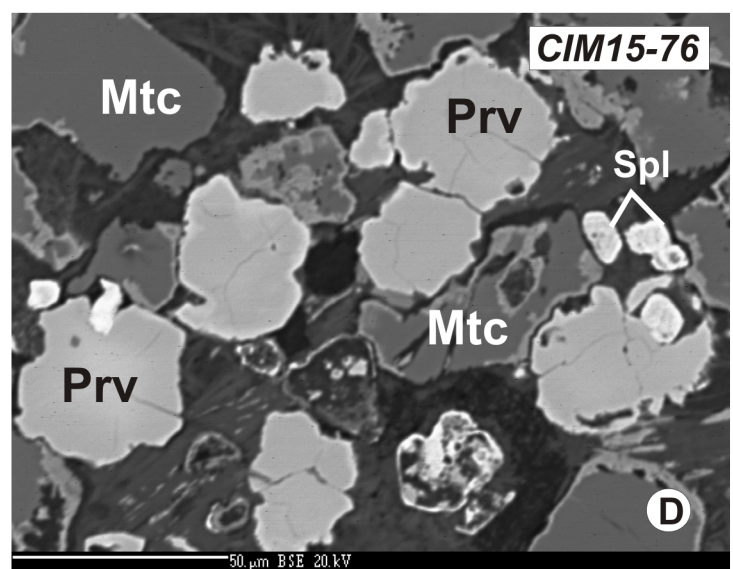
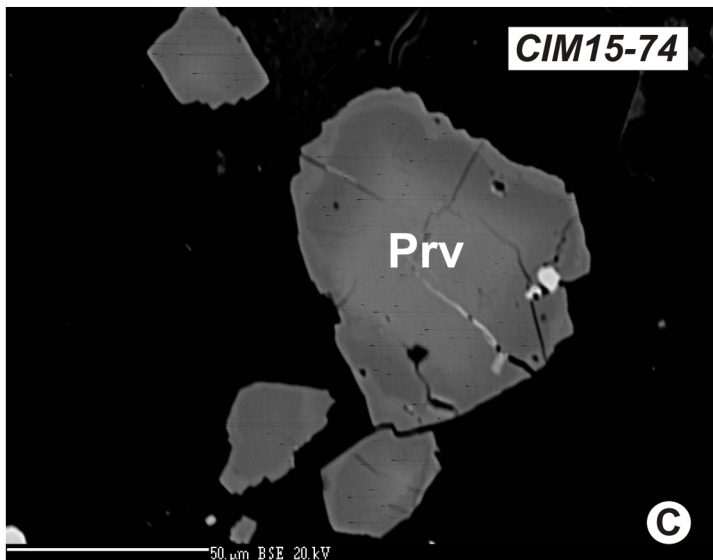
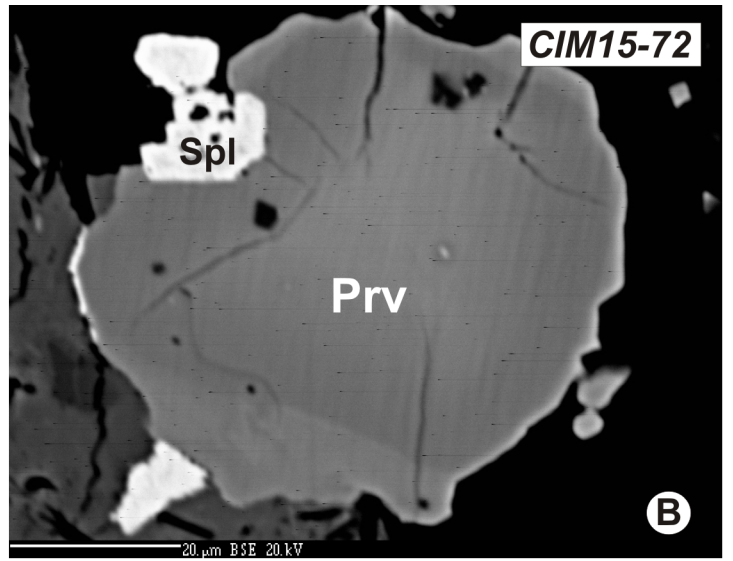
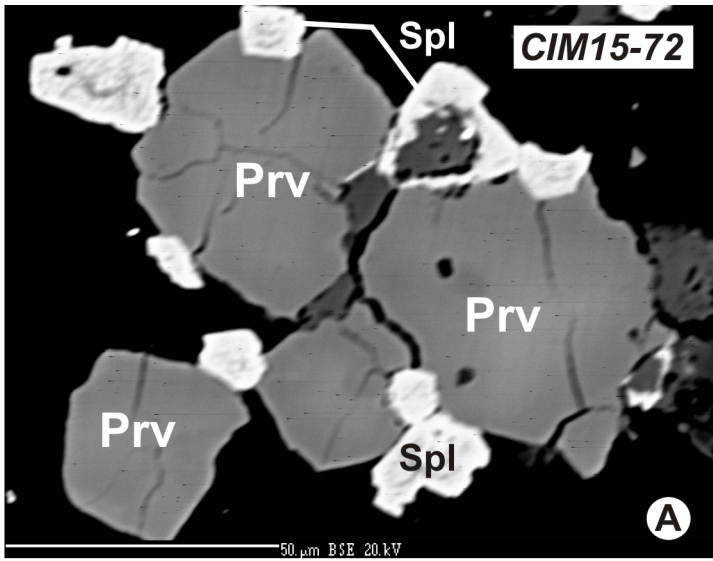
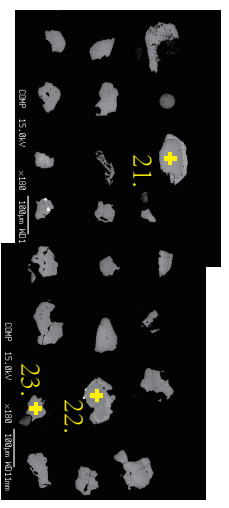
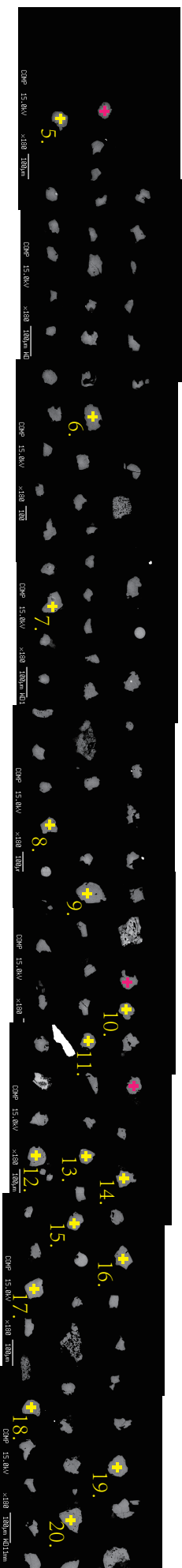
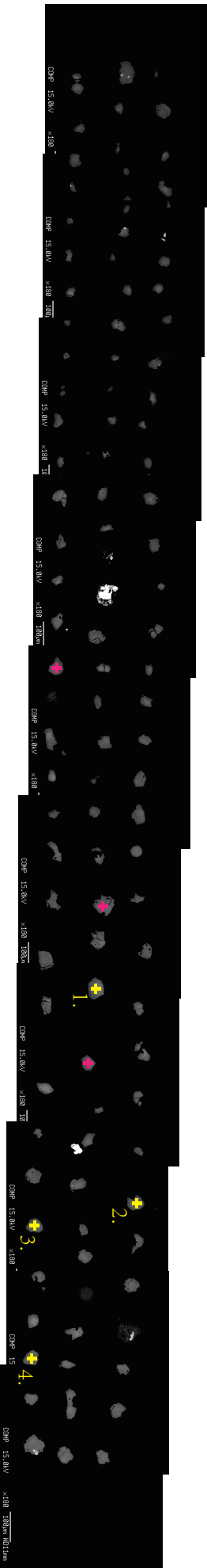


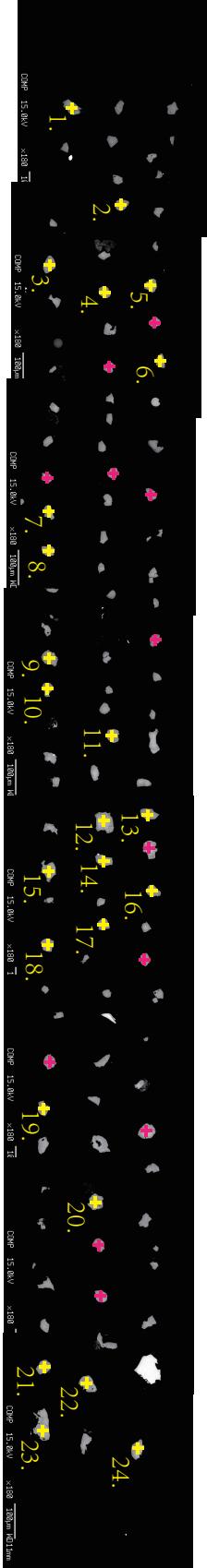
Figure DR4



BSE images
Mount# A4242
CIM15-072_Premier_Dyke (23 perovskite grains selected in yellow)



BSE images
Mount# A4242
CIM15-074_Premier_Dyke (24 perovskite grains selected in yellow)



BSE images
Mount# A4242

CIM15-076_Premier_Dyke (26 perovskite grains selected in yellow)

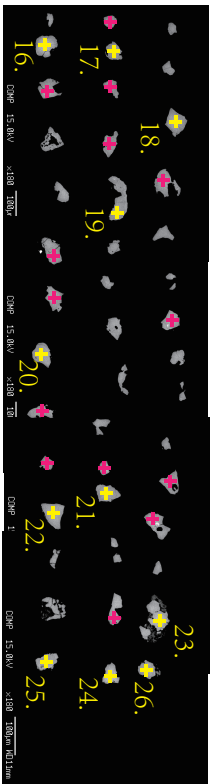
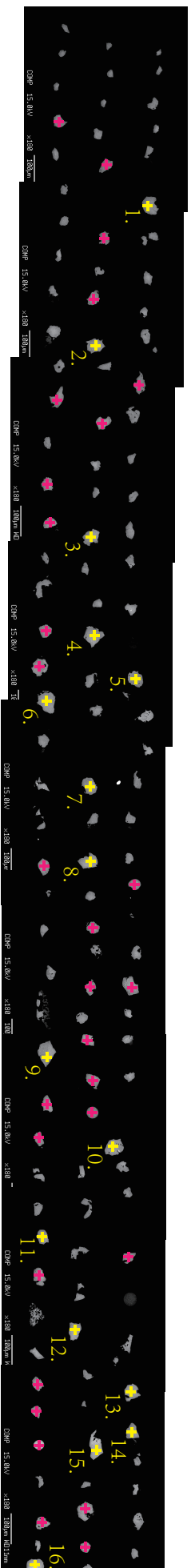


Figure DR5

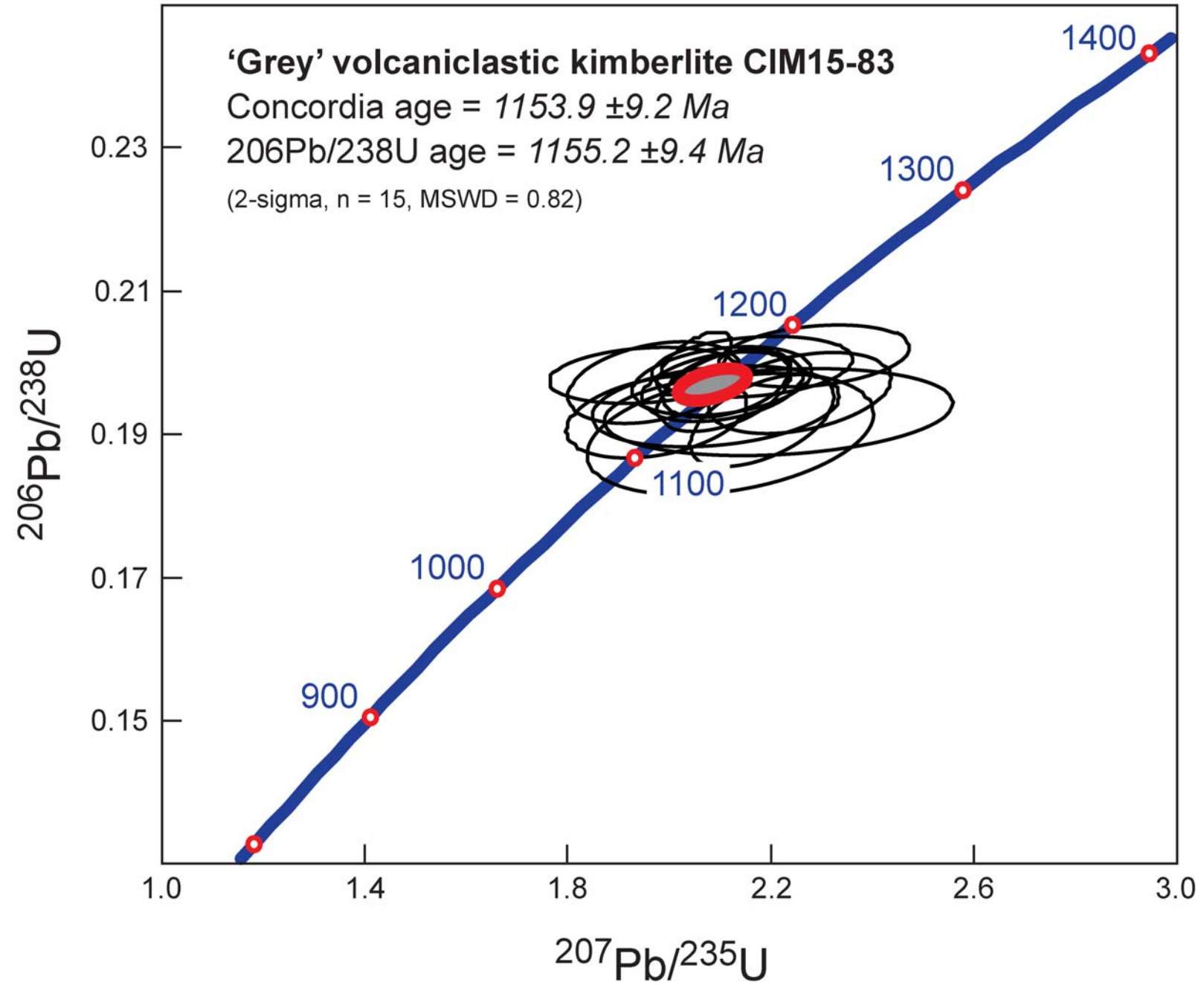
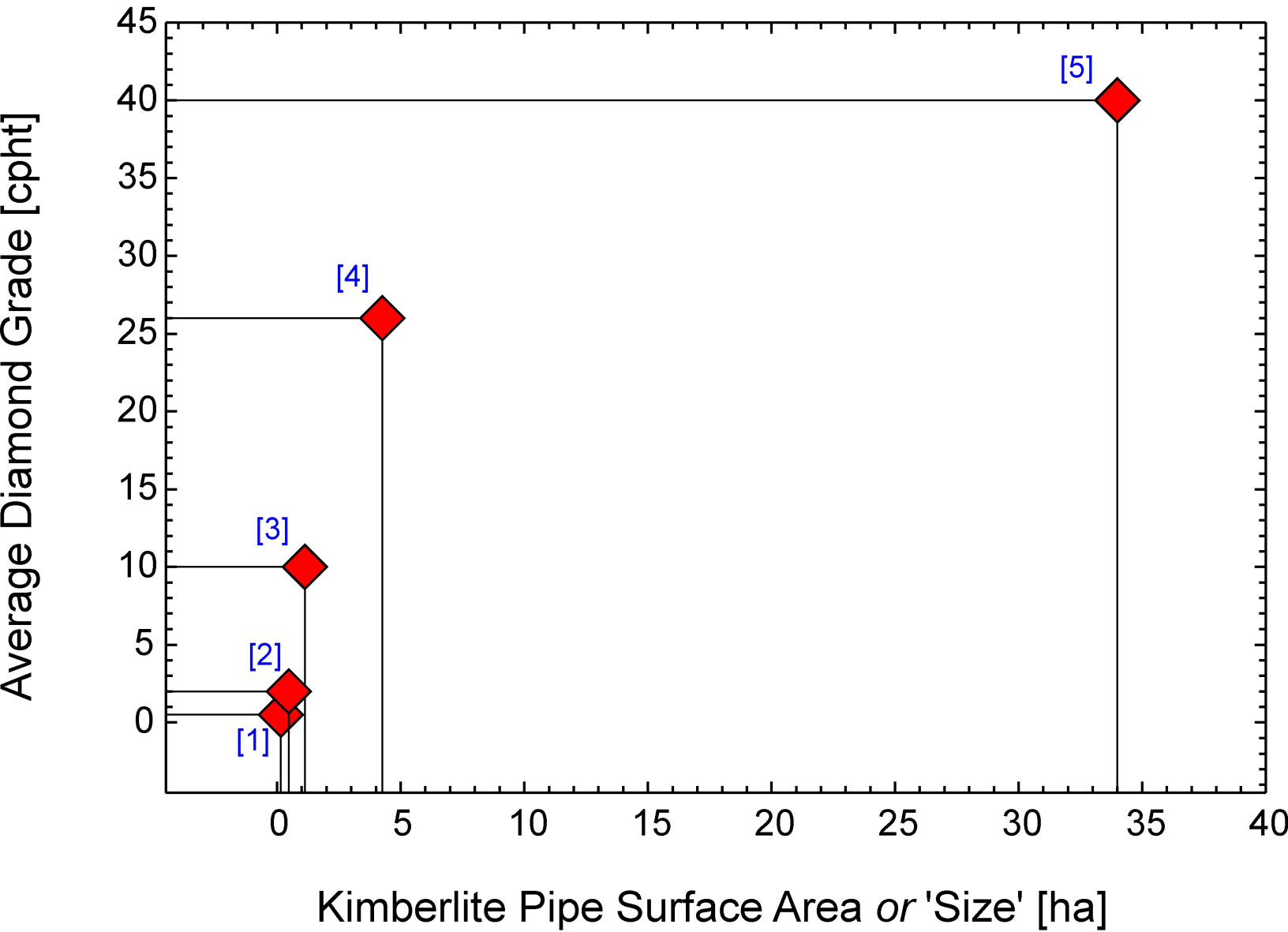


Figure DR6

◆ Premier kimberlite cluster (*South Africa*)



[1] Schuller Annexe

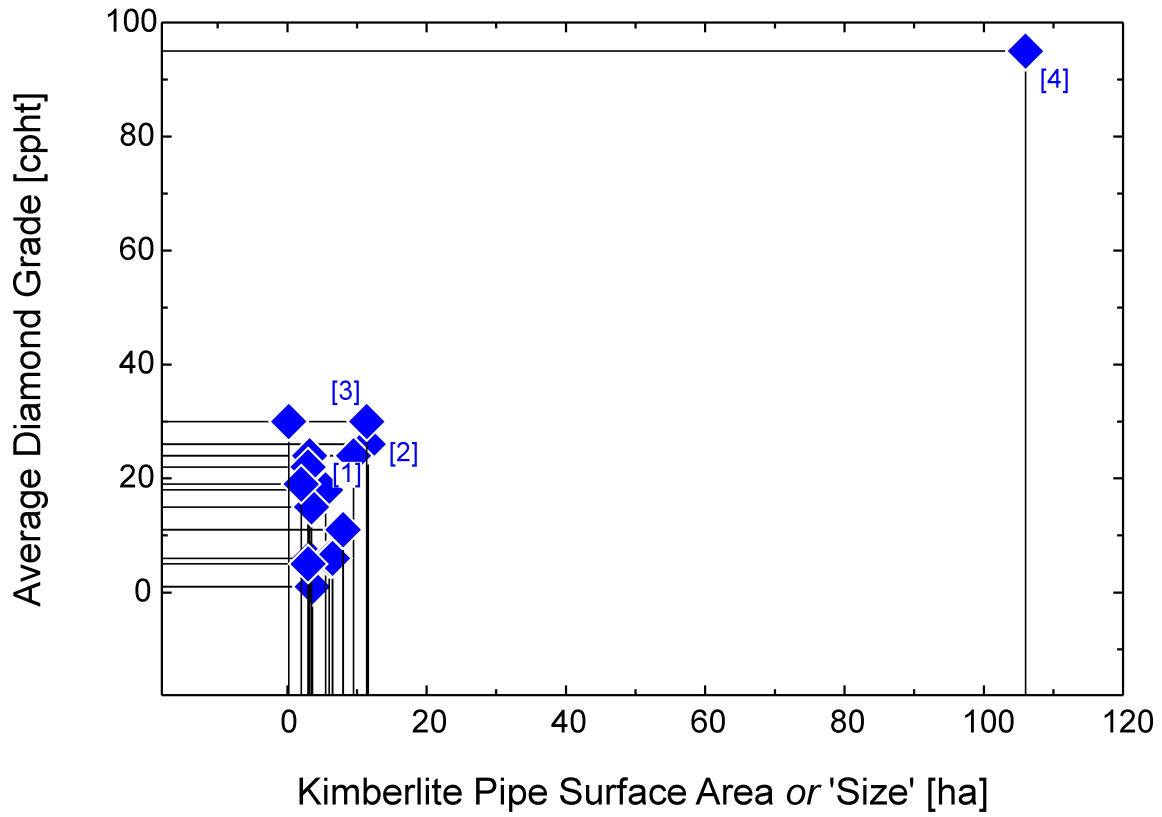
[2] National

[3] Schuller

[4] Montrose

[5] Premier / Cullinan Mine

◆ Orapa kimberlite field/cluster (*Botswana*)



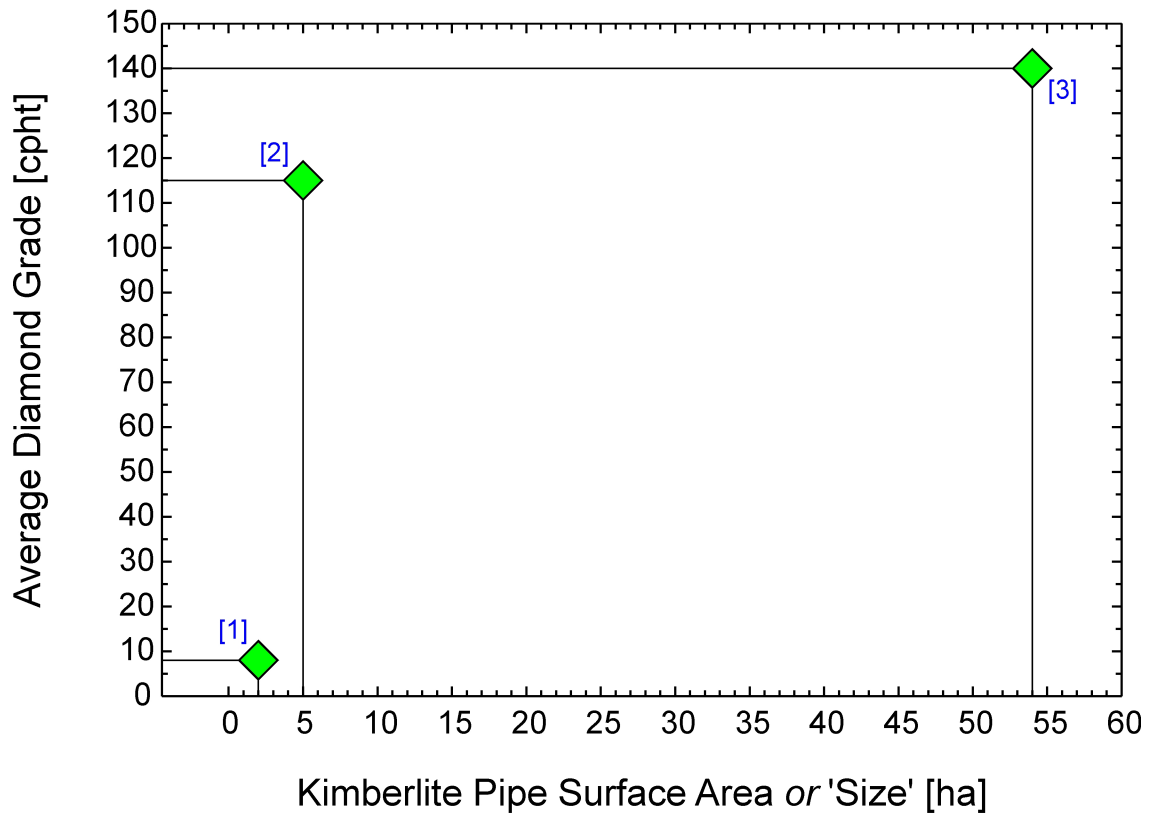
[1] AK6, Karowe Mine

[2] DK1, Letlhakane Mine

[3] BK9, Damtshaa Mine

[4] AK1, Orapa Mine

◆ Jwaneng kimberlite cluster (*Botswana*)

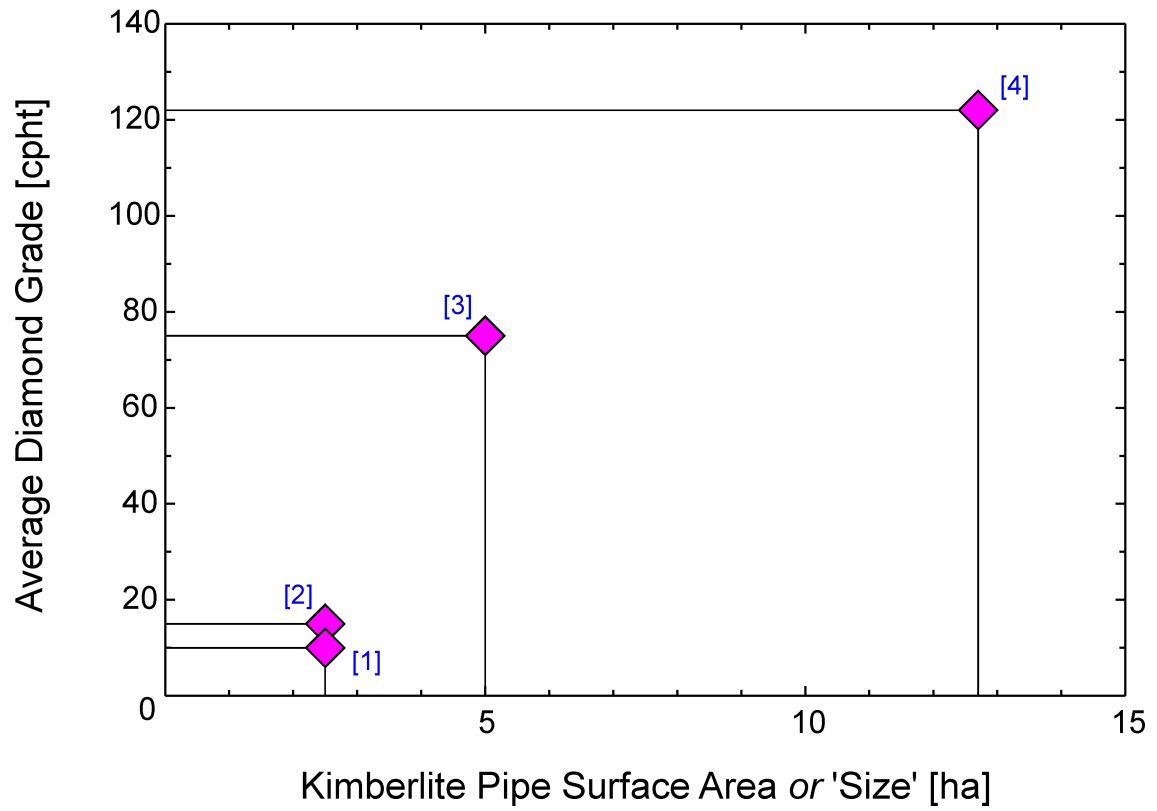


[1] DK12

[2] DK7

[3] DK2, Jwaneng Mine

◆ Venetia kimberlite cluster (South Africa)



[1] K04

[2] K03

[3] K02

[4] K01, Venetia Mine